Pure Appl. Geophys.

DOI 10.1007/s00024-014-1009-2

Pure and Applied Geophysics

A Threshold-Based Earthquake Early-Warning System for Offshore Events in Southern Iberia

M. Picozzi,[1] S. Colombelli,[1,2] A. Zollo,[1] M. Carranza,[3] and E. Buforn[3]

Abstract—The south of the Iberian Peninsula is situated at the convergence of the Eurasian and African plates. This region experiences large earthquakes with long separation in time, the best known of which was the great 1755 Lisbon Earthquake, which occurred SW of San Vicente Cape (SW Iberian Peninsula). The high risk of damaging earthquakes has recently led Carranza *et al.* (Geophys. Res. Lett. 40, 2013) to investigate the feasibility of an EEWS in this region. Analysis of the geometry for the Iberian seismic networks and the San Vicente Cape area led the authors to conclude that a threshold-based approach, which would not require real-time location of the earthquake, might be the best option for an EEWS in SW Iberia. In this work we investigate this hypothesis and propose a new EEW approach that extends standard P-wave threshold-based single-station analysis to the whole network. The proposed method enables real-time estimation of the potential damage at stations that are triggered by P-waves and those which are not triggered, with the advantage of greater lead-times for release of alerts. Results of tests made with synthetic data mimicking the scenario of the great 1755 Lisbon Earthquake, and those conducted by applying the new approach to available recordings, indicate that an EEW estimation of the potential damage associated with an event in the San Vicente Cape area can be obtained for a very large part of the Iberian Peninsula.

1. Introduction

An earthquake early warning system (EEWS) is a real-time system integrating a seismic network and software capable of performing real-time data telemetry and analysis to provide alert messages to users within seconds of the beginning of an earthquake and certainly before that the S-waves generated by the event reach the users.

Use of an EEWS to reduce exposure of populations to seismic risk is increasing, and several countries around the world have already developed EEWS, or are on the verge of doing so. Japan, Taiwan, Mexico, and California, for example, already have operational EEWSs (Horiuchi *et al.* 2005; Wu 2006; Espinosa-Aranda 2009; Böse *et al.* 2007, 2009). EEWSs are also under development and testing in other regions of the world, for example Italy, Turkey, and China (Satriano *et al.* 2011; Zollo 2014; Alcik *et al.* 2009; Peng *et al.* 2011). Finally, a feasibility study is in progress in Spain (Carranza 2013).

Most EEWS are designed as either "regional", "on-site", or "front-detection" systems. Selection of the configuration of the EEWS essentially depends on network geometry and source-to-site distance.

A regional warning system is based on a dense sensor network of stations deployed in the vicinity of a source region, whereas sites to be alerted are usually far from it. In this configuration, the earthquake location and magnitude are estimated by using the earliest recorded signals; peak ground motion at distant sites (peak ground velocity, PGV, or peak ground acceleration, PGA) is then predicted by use of empirical ground-motion prediction equations (e.g., among others, PRESTo in Southern Italy; Iannaccone *et al.* 2009; Satriano *et al.* 2011).

Site-specific (or onsite) EEWS consist of a single sensor deployed in the proximity of the target structure that is to be alerted. In this configuration, earthquake early warning (EEW) data measured in the very first seconds of the P-wave are used to predict the final peak ground motion at the same site, without locating the event or estimating its magnitude (e.g., among others, the τc-Pd Onsite algorithm in California; Böse *et al.* 2009, 2012).

The "front detection" approach consists of use of an array of seismic sensors between the potential source area and the target area. Such a system

[1] Department of Physics, Università Federico II, Naples, Italy. E-mail: matteo.picozzi@unina.it
[2] RISSC-Lab, AMRA scarl, Naples, Italy.
[3] Department Geofisica y Meteorogia, Univesidad Complutense, Madrid, Spain.

Published online: 18 December 2014

requires prior knowledge of the possible location of earthquake sources, but, depending on their distance from the target area, it can then provide quite long warning or lead times (i.e., tens of seconds) before arrival of destructive waves. An example of a front detection system is the seismic alert system (SAS) for Mexico City (Espinosa–Aranda *et al*. 1995), based on a linear array of sensors along the coast designed to detect earthquakes from the offshore subduction zone and to issue a warning to Mexico City.

Integrated approaches have also been proposed. The idea here is to jointly use both locally measured data and predicted ground motion on a regional scale. Integrated approaches are likely to provide reliable estimates of source parameters, to enable rapid prediction of the potential damage zone (PDZ) resulting from the earthquake (i.e., the area in which most of the damage is expected to occur), and to define local alert levels (Zollo *et al*. 2010; Colombelli *et al*. 2012a).

Whichever configuration is adopted, earthquake magnitude or peak ground motion estimates for early warning applications are based on empirical relationships between earthquake size and early P and S-wave train data (Kanamori 2005). In the context of real-time applications, use of different amplitude and period data have been proposed for obtaining independent estimates of the earthquake's magnitude. For prediction of ground shaking, which is usually described by use of a single variable (PGA or PGV), several authors have demonstrated that the maximum amplitude of the initial P-wave displacement (e.g., measured over the first 3 s) can be used as a proxy for the resulting PGV at the same site (Kanamori 2005; Wu 2005, 2008a, b; Zollo and Kanamori 2010).

The Iberian Peninsula is currently undergoing uniform NNW–SSE horizontal compression as a result of convergence of the Eurasian and African plates (Buforn *et al.* 1988a). The region situated at the plate boundary experiences large earthquakes with long return periods (Buforn *et al*. 1988b), and thus is of particular interest for an EEW study. The area of S. Vicente Cape (SVC, SW Iberia, Fig. 1) has generated large shocks, including the damaging 1755 Lisbon Earthquake and, more recently, the Ms 8.1 1969 S. Vicente Cape earthquake, both of which generated tsunamis. Moderate-to-strong earthquakes have also occurred in the Gulf of Cádiz (GC, Fig. 1),

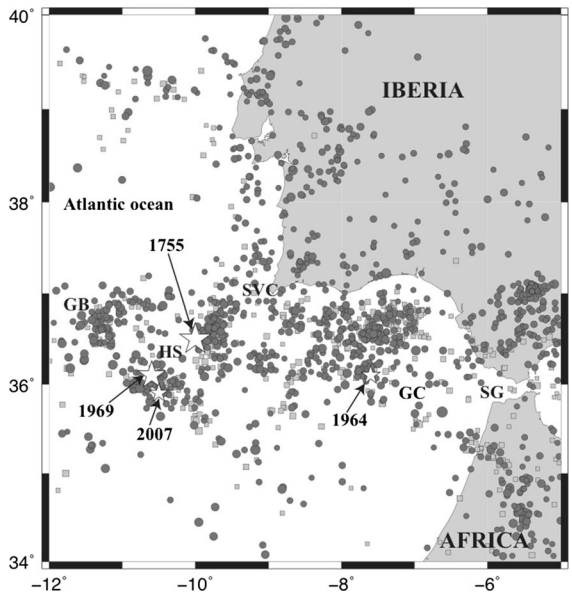

Figure 1
Distribution of earthquake epicenters ($M \geq 3$, period 1960–2014) taken from the Instituto Geográfico Nacional Data Base. *Black circles* correspond to shallow events ($h < 40$ km), *grey squares* to intermediate depth ($40 < h < 150$ km). *Stars* are the largest earthquakes. *GB* Gorringe Bank, *HS* Horsenhoe Scarp, *SVC* Saint Vicente Cape, *GC* Gulf of Cadiz, *SG* Strait of Gibraltar

an example being the Ms 6.1, 1964 event. In this area, however, earthquakes of even smaller magnitude can result in much panic and fear among the population, because they are felt over an extensive region; this occurred as a result of the December 2009 earthquake ($M_w = 5.5$), which was felt over a large part of the SW of the Iberian Peninsula, and as far away as its center (Pro *et al*. 2013).

Carranza (2013) investigated the feasibility of using an EEWS in these regions of the Iberian Peninsula, taking into account the limitations of existing seismological networks. The geometry of the Iberian seismic networks and the SVC and GC seismogenic zones makes it difficult to achieve early and reliable location of the epicenter. For this reason, Carranza (2013) suggested that a threshold-based approach, which would not require real-time location of the earthquake, might be the best option for an EEWS in SW Iberia. To better clarify this issue, we computed synthetic P-wave arrival times (corrupted by random noise with 1 s standard deviation) for a scenario mimicking the 1755 Lisbon Earthquake. We then tried to locate the event on the basis of different

numbers of stations and using the RTLoc algorithm of Satriano *et al.* (2008), one of the most robust algorithms developed within the EEW community. Figure 2a shows that when the first three stations only are used, the estimated location can be completely wrong. Figure 2b, c, in turn, show that the location found by use of ten stations considering two sets of arrival times varies as a function of the random noise added to the data. The latter examples, in particular, reveal that for this geometrical arrangement, and using a limited number of stations (which is a requirement in EEW operations), the inferred location is not reliable.

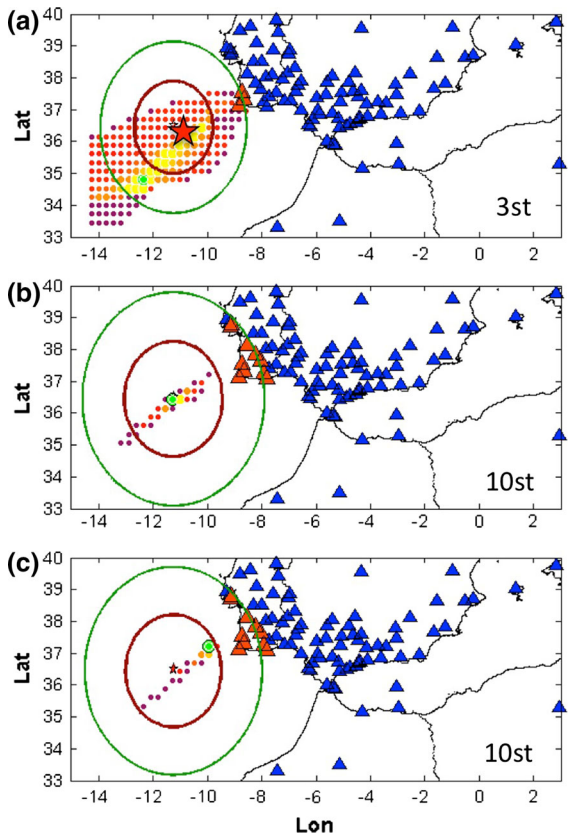

Figure 2
a Example of RTLoc-derived locations for an event mimicking the great 1755 Lisbon Earthquake (*red star*) for three triggered stations. The RTLoc solutions (*dots*) are of different colors, depending on their uncertainty (i.e., from *green*, indicating the best solution, to *violet* indicating the worst solutions). Triggered (*orange triangles*) and non-triggered (*blue triangles*) stations, P-wave (*green line*), and S-wave (*red line*) wavefronts are shown. **b** and **c**, the same as (**a**), but corresponding to use of ten triggered stations to derive the location and derived using two different sets of data

In this work, we investigated the hypothesis proposed by Carranza (2013). In particular, we proposed a new EEW approach that extends the standard on-site single station analysis scheme to the whole network. The purpose of the new approach is to estimate the potential damage at both stations that are triggered by P-waves, and at the non-activated stations. We exploit the EEW relationships derived by Carranza (2013) for SW Iberia. However, with regard to that study, in which only recordings from seismic stations with broad-band sensors were used, here we also considered strong motion stations (i.e., those of the Instituto Geográfico National (IGN), Western Mediterranean (WM), and Portuguese National (IP) networks), for a total of 112 stations, assuming that their hardware characteristics would enable real-time data telemetry. We also assumed that this seismic network would be managed at a major center, similarly to the ISNet network (Iannaccone *et al.* 2009), where the real-time data analysis necessary for EEW approach proposed in this study would occur.

2. *San Vicente Cape and Gulf of Cádiz Seismogenic Zones*

The San Vicente Cape (SVC) and Gulf of Cádiz (GC) seismogenic zones (Fig. 1) extend from 12°W to 6.5°W, and from 35°N to 37.5°N. A large number of papers have described these zones, which are of great interest because of their tectonic complexity and because they were the location of the occurrence of the great 1755 Lisbon Earthquake (Fukao 1973; Udías *et al*. 1976; Grimison and Chen 1988; Buforn 1988a; Morel and Megharoui 1996; Hayward *et al*. 1999; Fernández-Ibáñez *et al*. 2007; Stich *et al*. 2007; Pro *et al*. 2013). Buforn *et al*. (2015, this volume), describe in detail the largest earthquakes that have occurred in this region. The region's main characteristics may be described as follows (Fig. 1). Earthquakes are associated with the plate boundary between Eurasia and Africa, well defined at its western part, from the Azores Islands to 12°W. Along this longitude, a transition starts from an oceanic to a continental plate boundary. A consequence of this transition is that seismicity spreads over a wide area

and the plate boundary, which is not well defined, corresponds to a wide deformation zone that also includes the region south of Iberian Peninsula and northern Morocco.

Most of the epicenters within this zone are located offshore with three main concentrations of earthquakes (Fig. 1). The first is located in the western part of the region, at the Gorringe Bank (GB), in an NE–SW direction, in agreement with the trend of this structure. The second concentration is at the Horsenhoe Scarp (HS), where the 1969 ($M_w = 7.8$) and 2007 ($M_w = 5.9$) earthquakes occurred. This is one of the hypothetical locations of the epicenter of the 1755 Lisbon Earthquake. The third concentration corresponds to the Gulf of Cadiz (GC) where the 1964 earthquake ($M_s = 6.1$) occurred. On land, earthquakes are concentrated on both sides of the Strait of Gibraltar (SG), but with moderate magnitudes, usually less than 5.0.

Another characteristic of the earthquakes in these zones is their focal depth. Most epicenters correspond to shallow events ($h < 40$ km), but there are also earthquakes at intermediate depths ($40 < h < 150$ km, Fig. 1). Because of the poor azimuthal coverage of the seismic stations, determinations of focal depths are not well constrained and this intermediate-depth seismicity is uncertain (Buforn *et al*. 2004). However, it is important to note that for the 1969 and 2007 earthquakes, focal depths obtained from the inversion of body waves and slip distributions were between 30 and 40 km, whereas in the GC, the 1964 shock had a shallow focus (12 km).

Focal mechanisms of large earthquakes in the SVC and GC (1969, 2007, and 1964) correspond to a thrusting motion leading to a horizontal pressure axis oriented in the NNW–SSE direction, a consequence of the collision between the Eurasian and African plates.

3. Methodology

3.1. Overview

Figure 3 shows the outline of the EEW procedure we designed with the purpose of mitigating the seismic risk arising from the S. Vicente Cape area.

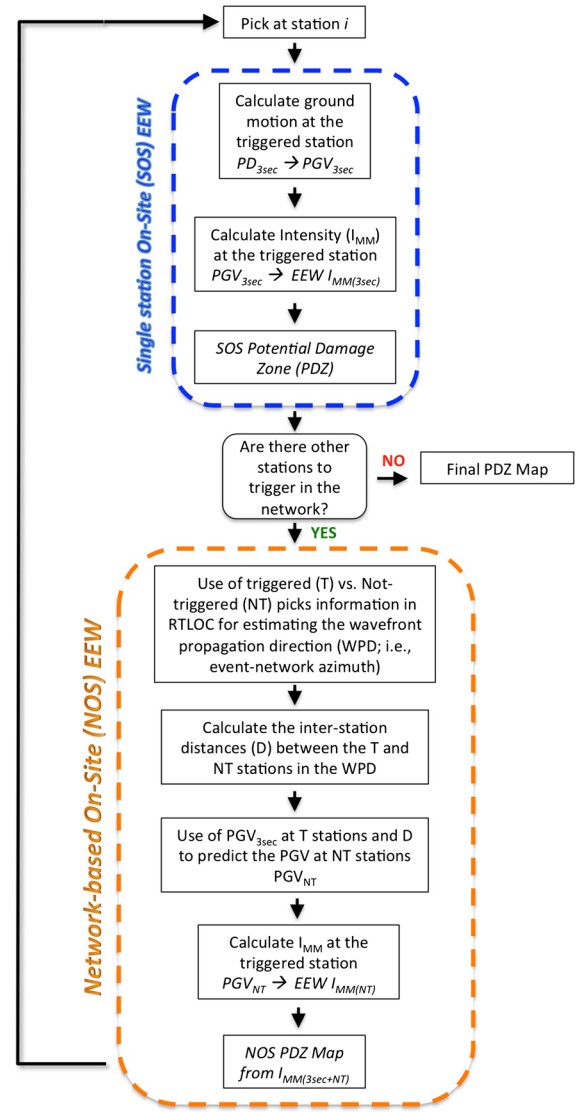

Figure 3
Outline of the EEW procedure proposed for the Iberian Peninsula to deal with the seismic threat arising from the SVC and GC areas

As discussed in the previous section, given the geometrical relationship between the S. Vicente Cape source area, the seismic network, and the distribution of the cities (i.e., the EEWS's targets), we opted for a threshold-based EEW approach, with the intention of predicting the potential damaging effects of an offshore earthquake by real-time analysis of signals recorded by coastal stations without any need for accurate estimation of earthquake location and magnitude. The procedure is composed of two main parts.

The first consists of a classical single station on-site approach (SOS). The empirical scaling relationship between the initial peak ground displacement (Pd) and the final peak ground velocity (PGV) at each recording site is one of the most stable and robust correlations used for EEWS (Wu 2005, 2008a, b; Zollo and Kanamori 2010). The Pd is typically measured in a three-second window after arrival of the first P-wave. Colombelli *et al.* (2012b, 2014) recently showed that an expanded P-wave time window should be used to overcome the Pd saturation effect for large earthquakes (i.e., $M > 7$; e.g., among others, Rydelek and Horiuchi 2006; Rydelek *et al.* 2007; Zollo and Nielsen 2007).

We apply the log Pd as a function of PGV empirical relationship derived by Carranza (2013). The PGV predicted from Pd (PGV_{3sec}) is, in turn, then converted to a modified Mercalli intensity (I_{MM}) by use of the empirical regression proposed by Wald *et al*. (1999), which is implemented by the USGS in the Shake Map tool for rapid estimation of strong ground shaking after a damaging earthquake. Thus, the potential damaging effects of a moderate-to-large earthquake can be rapidly predicted by Pd measurements by using the correlation of this variable with PGV. Hence, as proposed by Zollo and Kanamori (2010) and Colombelli *et al.* (2012a), the I_{MM} derived from the recorded P-waves can be used to deliver a potential damage zone (PDZ) map. When such a SOS approach is used, estimation of I_{MM} is possible only at stations already triggered by the P-waves.

To also achieve prompt estimation of potential damage at sites not yet reached by the P-waves, we propose here an approach in which the information derived by the SOS scheme is integrated with information describing the geometrical relationship between triggered and non-triggered stations. We term the second procedure the "network-based on-site approach" (NOS), the objective of which is prediction of I_{MM} at non-triggered stations.

As shown in Fig. 3, the SOS approach is adopted whenever another station is triggered and a local P-wave prediction of the final I_{MM} at that site is derived. The procedure continues delivering evolutionary maps of the predicted shaking at the station sites until no more non-triggered stations are left. In accordance with Zollo and Kanamori (2010), the I_{MM} maps can be used to derive the PDZ. Whenever coastal stations begin recording the S-wave ground motion, these pieces of information can then be included within the NOS procedure for prediction of the shaking at non-triggered stations for any other target of interest.

3.2. Network-Based On-Site (NOS) Approach

For offshore earthquakes, the network-based on-site (NOS) approach exploits real time information from triggered and not-yet-triggered stations to constrain the direction of propagation of the P-wave-front (Fig. 4a), and therefore the epicenter back-azimuth. For this purpose, a simplified version of the RTLoc algorithm of Satriano (2008) was adopted. The information provided at a given instant (t_{now}) during the initial stages of an earthquake, that is when the network status involves a few triggered stations and some non-triggered, can be used to compute the "conditional" equal differential (EDT) surfaces (Font *et al*. 2004). As discussed by Satriano (2008), these EDT surfaces are conditional because they are defined under the condition that for each pair of triggered and non-triggered stations, the latter will trigger at any time after the current clock time t_{now}.

Figure 4b–d show an application of this evolutionary procedure to synthetic data derived for a scenario having the epicenter corresponding to the 1755 Lisbon Earthquake. All the synthetic P-wave arrival times used in this work, which are necessary for implementation of the RTLoc algorithm, have been computed for a 1D velocity model for the South Iberia region (IGN 1983), with noise introduced consisting of a random perturbation with a standard deviation equal to one second. With the passing of time, the progressive increase in the number of triggered stations enables improved identification of the region in which the epicenter is most probably located. Then, knowledge of the P-wavefronts' direction of propagation enables assessment of the interstation distances (D) between triggered and the non-triggered stations (Fig. 4b), which in turn is a fundamental piece of information for estimating the PGV at non-triggered stations. Because the true location of the epicenter is unknown, and for the SVC

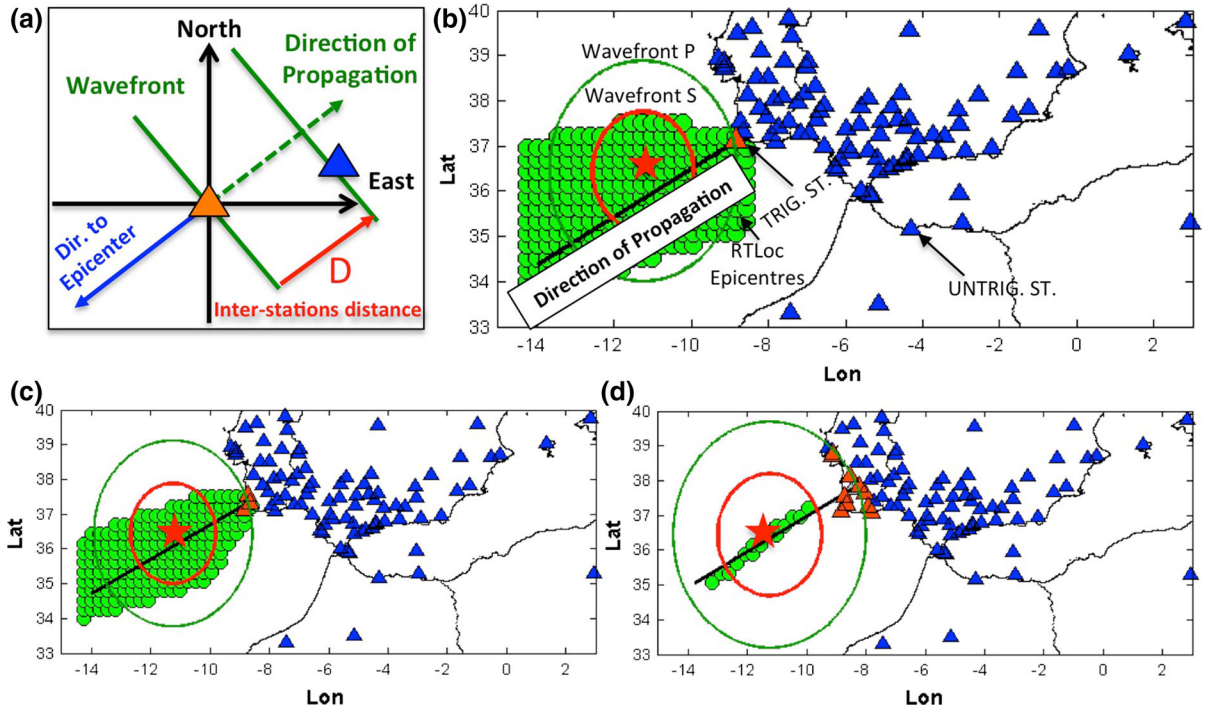

Figure 4

a Schematic illustration (*horizontal plane*) of a wavefront propagating across two stations, and derivation of inter-station distance. **b** Example of the application of a simplified RTLoc where only solutions compatible with the "conditional" EDT are shown (*green dots*) when one station (*orange triangle*) has been triggered. The true location (*red star*) and the estimated direction of propagation of wavefronts (*black line*) are also shown. **c** and **d**, the same as (**b**), but at the moment when three and ten stations, have been triggered, respectively

and GC areas their distance from the coast is large, the interstation distances are estimated with the assumption of planar wavefronts.

Similarly to the EEW procedure for the Pd (Zollo *et al.* 2006), PGV is related to the earthquake magnitude (M) and the hypocentral distance (R) by using a standard ground motion prediction equation (GMPE):

$$\log_{10}(\mathrm{PGV}) = A + B \times M + C \times \log_{10}(R) \quad (1)$$

where PGV is in centimeters per second, R is in kilometers, and A, B, and C are constants to be determined by a multivariate linear regression analysis of data for the specific region.

Use of Eq. (1) within the NOS procedure to determine the PGV at non-triggered stations is, however, not possible, given that R is not known.

However, on the basis of the observed decay of PGV with distance from the first triggered station (D), we propose the following attenuation model:

$$\log_{10}(\mathrm{PGV}_{3\mathrm{sec}})_D = \mathrm{So} + C' \times \log_{10}(D) \quad (2)$$

where C' is assumed to be equal to C (the validity of this assumption was verified for available recordings, as discussed in the section "Application and Preliminary Results" and illustrated in Fig. 5), and the term "So" is determined in real time by use of the best-fit regression expressed by Eq. (2) using the $\mathrm{PGV}_{3\mathrm{sec}}$ measured at the triggered stations and using their distances (D) measured along the wavefront's propagation direction from the first-triggered station.

Hence, when the wavefront's propagation direction is known, Eq. (2) can be used to estimate the PGV at non-triggered stations ($\mathrm{PGV}_{\mathrm{NT}}$). The procedure used to estimate the factor (So) and $\mathrm{PGV}_{\mathrm{NT}}$ can start when at least two PGV values are available (i.e., two triggered stations), and is repeated every time another station is triggered and its $\mathrm{PGV}_{3\mathrm{sec}}$ value is available (Fig. 5a). Therefore, similar to determination of the azimuth, estimation of the $\mathrm{PGV}_{\mathrm{NT}}$ is also

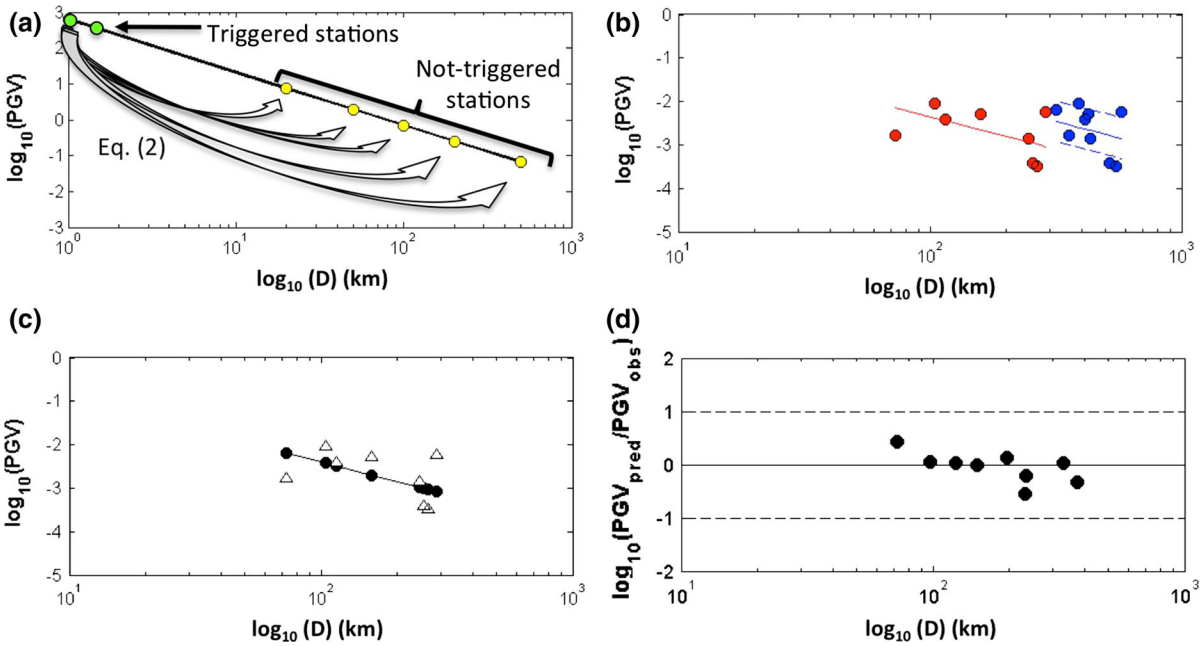

Figure 5

a Schematic illustration of PGV estimation at non-triggered stations (*yellow dots*) given at least two triggered stations (*green dots*) and the interstation distance between them and the others. **b** Comparison of PGV for event #6 *plotted* with respect to both their epicentral distance (*blue dots*) and their interstation distance (*red dots*) together with Eq. (3) (*blue line*) and Eq. (2) (*red lines*). **c** Comparison of observed (*white triangles*) and predicted (*black dots*) PGVs. **d** Residuals computed between the observed and predicted PGVs

evolutionary, and continues until all the stations in the network have been triggered (Fig. 3).

At each time a new or updated PGV_{NT} estimate is available, the empirical regression law proposed by Wald *et al.* (1999) is used to estimate the $I_{MM(NT)}$. Hence, a PDZ map, including the $I_{MM(3\ s\ +\ NT)}$ values that cover the whole area monitored by the seismic network, is computed (Fig. 3). Of course, with the passing of time, the NOS-derived intensity map will evolve to include more observed S-wave and Pd-derived PGV values.

In principle, the procedure can be easily extended to any EEW target of interest.

4. Application and Preliminary Results

We tested the above EEW procedure for the S. Vicente Cape area using both synthetic and real data. The use of synthetic data was necessary because of a lack of recordings for larger earthquakes ($M > 6$) in the area under study. The available real recordings are in fact relevant to seven moderate earthquakes (i.e., M between 4.5 and 5.9; Table 1), which were the largest events among those considered by Carranza (2013) to derive, for the South Iberia Region, the empirical scaling relationships between Pd, M, and R, and between Pd and PGV.

Table 1

Main information of the recorded events with epicenters in the SVC and GC seismogenic regions considered in this study

Id	Date	Time	Lat	Lon	Depth	M_w
1	10/01/2006	10:57:40	36.15	−7.71	40	4.7
2	21/06/2006	00:51:19	35.99	−10.63	40	4.9
3	12/02/2007	10:35:24	35.91	−10.46	30	5.9
4	10/05/2008	16:33:09	35.95	−10.75	40	4.7
5	22/05/2009	23:58:06	36.77	−9.79	40	4.5
6	05/07/2009	15:50:56	36.00	−10.48	35	4.5
7	17/12/2009	01:37:49	36.47	−10.03	35	5.5

Because we did not find in the literature a GMPE for computing the PGV at the epicentral distances of interest (i.e., between 100 and 600 km), we combined the relationships derived by Carranza (2013) in a new standard attenuation expression that relates PGV with M and R (see Eq. 1):

$$\log_{10}(\mathrm{PGV}) = -2.76 + 0.887 \times M - 1.479 \times \log_{10}(R) \quad (3)$$

Figure 6a shows, as an example, comparison of Eq. (3), with curves representing plus and minus one standard deviation, and the PGV measured for event #6 in Table 1. Figure 6b, c show, for all the events considered in this study (Table 1), that the prediction errors (i.e., the logarithm of the ratio of the predicted PGV value to the observed value) plotted against epicentral distance (Fig. 6b), and the relevant histogram (Fig. 6c), are stable over time, with maximum variability of approximately ±1, which is comparable with the usually encountered fluctuations in standard GMPEs (Akkar and Bommer 2007). These results suggest that the distance attenuation coefficient of Eq. (3) can be used to predict the PGV at large distances within the Iberia region by use of Eq. (2), by following the procedure described in the section "Network-Based On-Site (NOS) Approach".

Figure 5b shows the PGV observation for event #6 (Table 1) plotted both relative to their epicentral distances and their interstation distances, together with the curves from Eqs. (3) and (2), whose variables were found by following the procedure described in the section "Network-Based On-Site (NOS) Approach". For the same data, Fig. 5c, d show a comparison of the observed and predicted PGV values (i.e., from Eq. 2) and prediction errors as a function of interstation distance. These results indicate that Eq. 2 and the procedure described in the section "Network-Based On-Site (NOS) Approach" enable prediction of reliable $\mathrm{PGV_{NT}}$ values, despite not knowing the epicentral distance.

4.1. Synthetic data scenario

To perform a first validation of the EEW procedure for a scenario mimicking the ground motion associated with the great 1755 Lisbon Earthquake (M_w 8.7), we used synthetic data. The input data are Pd values computed by use of the relationship derived by Carranza (2013) considering the epicentral location and magnitude associated with this historical event (Johnston 1996; Martínez Solares 2004), and the current network configuration (Fig. 2). To make the feasibility tests more realistic, random noise is added to the Pd values, by considering the standard deviation associated with the relationship, and, hence, they are expected to represent the actual ground motion variability in the real data.

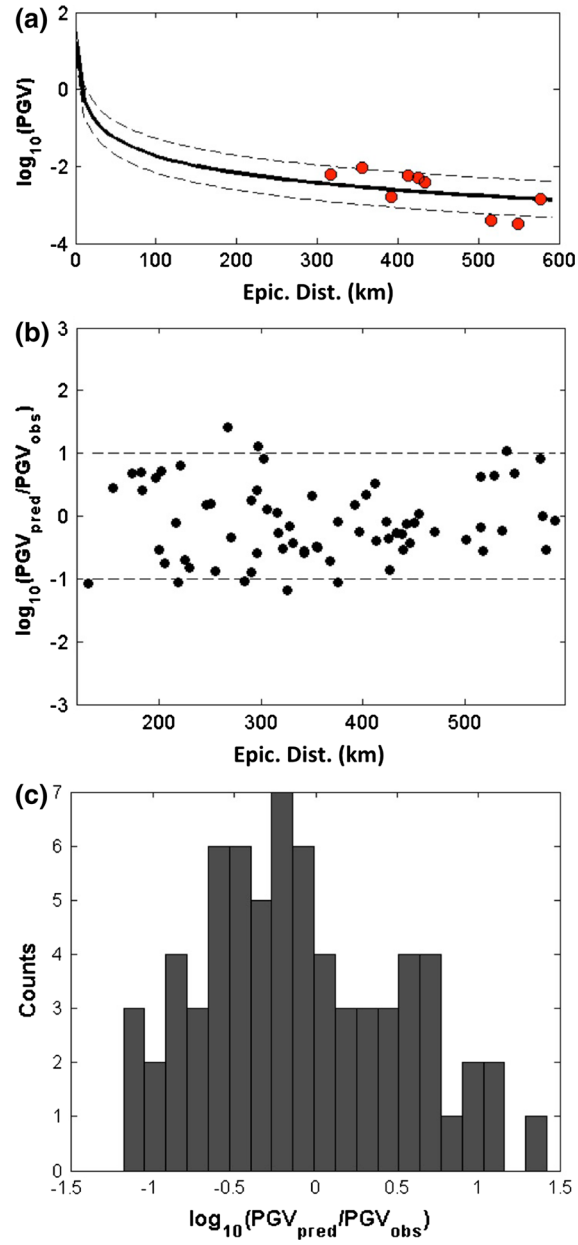

Figure 6
a PGV-GMPE (*black line*) derived from the EEW relationship of Carranza (2013), with the ±1 standard deviation curves (*dashed lines*) and the observed PGVs for event #6 (Table 1) whose epicenter is in the SVC region. **b** and **c** Distribution distance and histogram, respectively, of the residual between the observed and predicted PGVs from the recordings of the seven events considered in this study (Table 1)

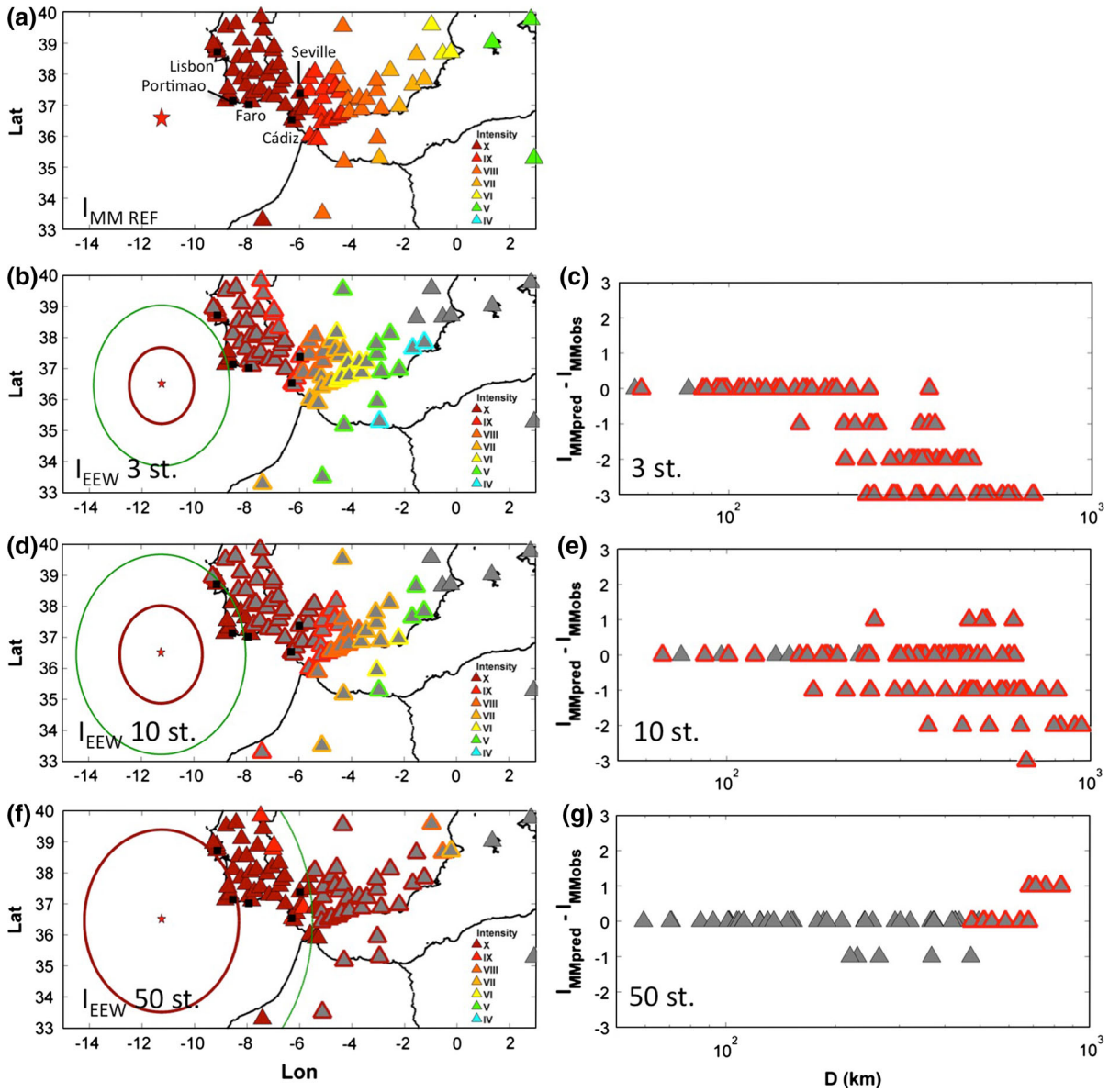

Figure 7

a I_{MM} derived from PGVs for a scenario mimicking the great 1755 Lisbon Earthquake. Seismic stations (*triangles*) are colored according to the I_{MM} scale of WALD *et al.* (1999). Target cities (Table 2) are shown as *black squares*. **b** I_{MM} at triggered stations from the SOS procedure (*full colored triangles*), and at non-triggered stations from the NOS procedure (*contour colored triangles*) at the time when three stations have triggered. **c** Distribution with distance of residuals between observed and predicted I_{MM} values. The stations have a different contour color depending on whether they are triggered (*black*) or not triggered (*red*). **d** and **f**, the same as (**b**), but for ten and fifty triggered stations, respectively, **e** and **g**, the same as (**c**), but for ten and fifty triggered stations, respectively

Figure 7a shows the map of reference intensities derived by the PGV from Eq. (3) for the location and magnitude of the 1755 Lisbon Earthquake and the WALD *et al.* (1999) relationship. Figure 7b shows the I_{MM} obtained by application of the SOS and NOS procedures when the first three stations have triggered. For clarity, in all the following figures we have adopted a different formalism while drawing the I_{MM} for triggered and non-triggered stations (i.e., fully and contour colored symbols, respectively).

Table 2

Lead-times for some Portuguese and Spanish target cities at the moment when different numbers of stations have been triggered by P-waves for the 1755 Lisbon Earthquake (Fig. 7)

City	Lead-time 3 stations (s)	Lead-time 10 stations (s)	50 Stations (s)
Cádiz	73	65	38
Faro	41	33	5
Lisbon	43	35	8
Portimao	29	21	0
Seville	82	73	46

Furthermore, as an example, we have computed the lead-time for some Portuguese and Spanish target cities (Table 2; Fig. 7a). In particular, the lead time has been computed as the S-wave arrival time at the target cities minus both the P-wave arrival time at a given triggered station (i.e., the 3rd, 10th, and 50th stations as in Fig. 7b, d, f) and a time of 2 s which is necessary for computation and data telemetry, which we assumed according to the experience with the PRESTo system at the ISNET accelerometric network in Southern Italy over a long period of testing (Satriano *et al.* 2011).

For the example with the three triggered stations (Fig. 7b), the lead-time at the selected targets would potentially range between a minimum of 29 s for Portimao, and a maximum of 82 s for Seville (Table 2).

Figure 7c shows residuals between reference and estimated I_{MM} values as a function of inter-station distance. This result indicates that at this time, the estimate of $I_{MM(NT)}$ is stable until about 200 km from the triggered stations. For larger distances, the NOS procedure has a bias toward smaller values by approximately three intensity units. However, by the time ten stations have triggered (Fig. 7d), the EEW I_{MM} map is more consistent with the reference map, with the residuals mostly confined within a range of ±one intensity unit. In this case, given the large source-to-target distances involved, the lead-time at the target cities is still large and ranges between 21 s for Portimao, and 73 s for Seville.

With the increase in the number of triggered stations, the EEW I_{MM} map relies much more on the PGV values derived from the SOS approach (i.e., from Pd values) and progressively improves its fit with the reference one, of course at the price of a reduction in the lead-time. This is shown, for example, in Fig. 7f, g, which are derived on the basis of fifty triggered stations, leading to no lead-time for Portimao, 5 s for Faro and 46 s for Seville.

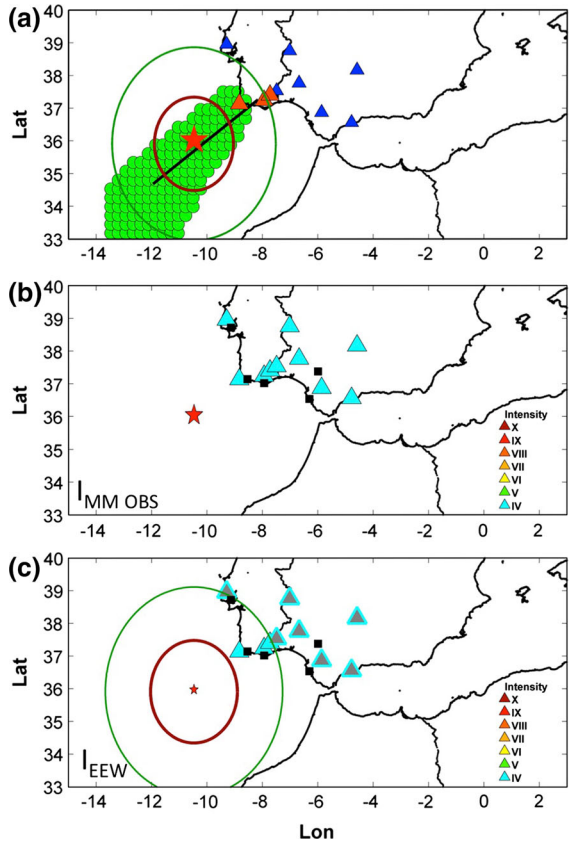

Figure 8
a The same as Fig. 4a, but for event #3 (Table 1). **b** and **c** are the observed and EEW I_{MM} values, respectively. The symbols are the same as in Fig. 7

4.2. Observed Data Analysis

The proposed EEW procedure was then applied offline to a set of recordings from seven small-to-moderate offshore earthquakes (Table 1). Of course, given their epicentral distances from the coast of approximately one hundred kilometers, and being of rather low magnitude (only in two cases larger than 5), the observed ground motion at the seismic stations is relatively small, and I_{MM} is less than V at all sites. In Fig. 8, we present the results of the EEW analysis for the 2007 (M 5.9) event, which occurred in the S.

Table 3

Lead-times at some Portuguese and Spanish target cities for the M 5.9 (#3), M5.5 (#7), and M 4.7 (#1) events (Table 1; Figs. 8 and 9)

City	Ev. #3 (s)	Ev. #7 (s)	Ev. #1 (s)
Cádiz	54	52	8
Faro	25	21	0
Lisbon	43	36	52
Portimao	16	9	7
Seville	65	62	27

Vicente Cape area (#3, Table 1). Interestingly, when using real data, after only three stations have been triggered, the EEW I_{MM} map is in agreement with the observed one according to the IGN (http://www.ign.es/ign/layoutIn/sismoDetalleTerremotos.do, last accessed on July 15, 2014). The resulting lead-times at the target cities range from 16 to 65 s (Table 3). In addition, despite their very low magnitudes, because of the different sources, we also considered the cases of the M5.5 (#7) and M 4.7 (#1) events (Table 1), which occurred in the Gulf of Cadiz (Fig. 9). Again in these cases, by the time three and two stations, respectively, have triggered, we observe good agreement between the observed and predicted EEW intensity maps. Moreover, with the only exception being the city of Faro for event #1 (Fig. 9f), the lead-time is still greater than zero (Table 3).

5. Discussion

In the previous section, we considered the SVC seismogenic region and presented a new EEW P-wave threshold-based approach for SW Iberia, where a classic Pd-PGV single-station analysis is extended to the whole network with the purpose of rapidly deriving a PDZ map for the Iberian Peninsula.

Existing GMPEs are mostly limited to a distance range of one hundred kilometers (Akkar and Bommer 2007; Bindi *et al.* 2010). For large events, however, for example the 1755 Lisbon Earthquake, these relationships are not appropriate for estimating the PGV at the large hypocentral distances in SW Iberia (i.e., mostly greater than two hundred kilometers). For this reason, we exploited the EEW relationships derived by Carranza (2013), which cover a distance range up to six hundred kilometers, to derive a new PGV attenuation law (Eq. 3). One limitation of this law, and therefore the method we propose, might be that the maximum magnitude of the events contained in the data set used by Carranza (2013) was only 6.3. In our opinion, considering the high seismic risk of the Iberian Peninsula with regard to the occurrence of a great earthquake in the SVC region, the capability to predict the ground motion at large distances is an issue of primary importance that deserves further study.

For such a seismic threat, we believe the most suitable EEWS for SW Iberia is a front-detection, threshold-based approach that exploits the information acquired at coastal stations to warn coastal sites and inland regions. As Carranza (2013) and our study have shown, the early seconds of P-wave recordings can be used to achieve, in a very short time, robust prediction of the PGV at the recording stations. Information dealing with the expected ground shaking at these stations could then be communicated to the inland areas. Of course, because of a lack of knowledge about the event's location and magnitude, estimation of the damage potential would usually be possible only for stations that recorded the P-waves and not for the others. With regard to this issue, the procedure that we propose in this work takes a step forward in enabling prediction of the potential damage at stations that have not yet recorded the P-waves (i.e., by use of Eq. 2), resulting the advantage of a greater lead-time for release of alerts. Furthermore, the method could be used to provide potential damage estimation for any specified target area in the region.

We used synthetic data to mimic the scenario of the great 1755 Lisbon Earthquake. Our results indicate that by use of only ten triggered coastal stations, a robust estimate of potential damage, expressed as I_{MM}, can be obtained for a very large portion of the Iberian Peninsula. These results have were obtained by using, as input data, Pd randomly extracted from the regression between this variable, M, and R. Therefore, differently from use of real Pd values measured with short-time windows, our synthetic data do not suffer from the well-known saturation problem of EEW variables. We are, however, well aware that this issue cannot be ignored when real data are considered. Therefore, to be effective for great

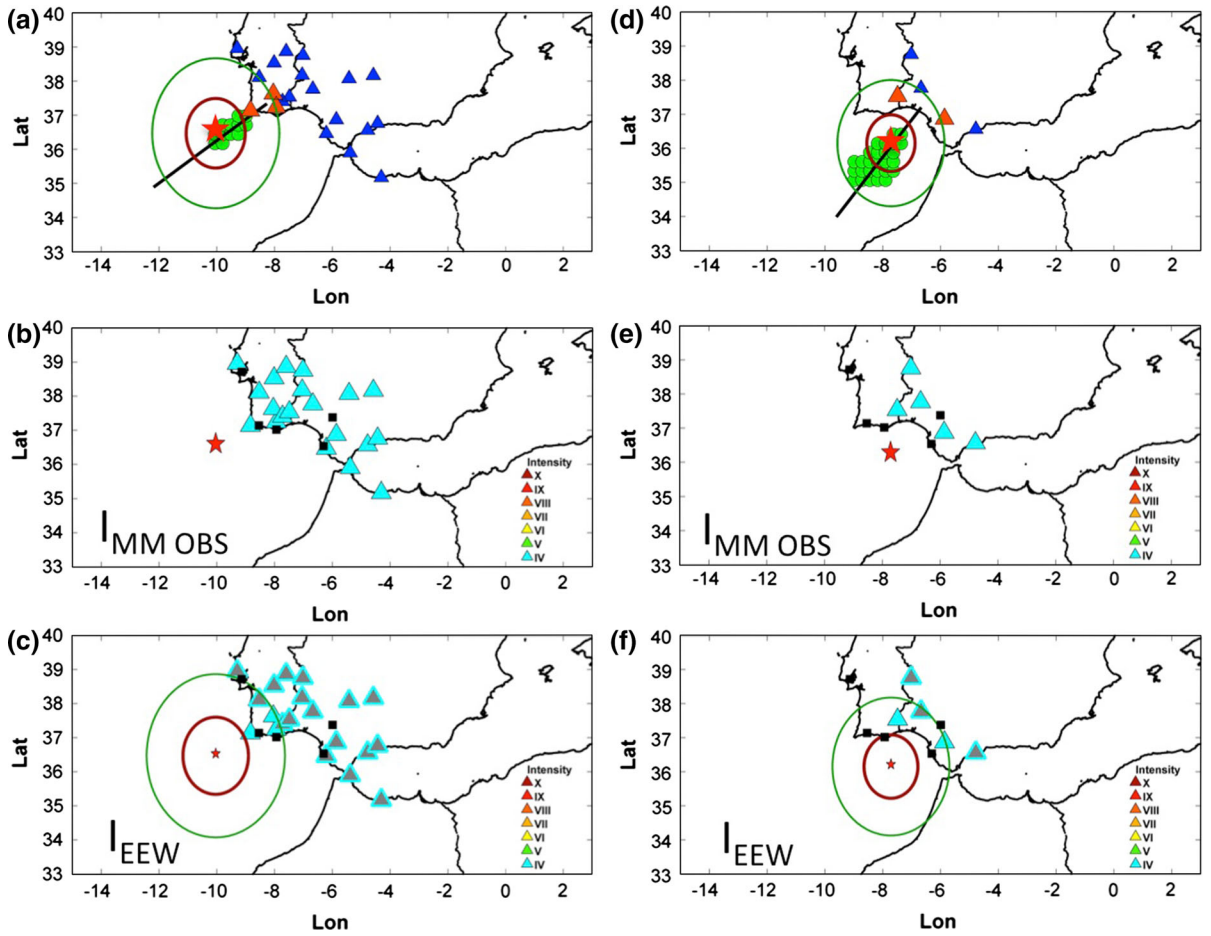

Figure 9
The same as Fig. 8, but for event #7 (**a**, **b**, and **c**), and event #1 (**d**, **e**, and **f**) of Table 1

events, the procedure we propose should include estimation of Pd from evolving, increasing P-wave time windows as proposed by COLOMBELLI *et al.* (2012b, 2014).

Although the waveform data set analyzed included data for low to moderate magnitude events only, we consider the results from application of our EEW procedure very encouraging. We have already shown that from the EEW information extracted from the first two or three triggered stations, reliable warnings accompanied by quite large lead-times can be released to rather large areas in the event of an earthquake in the SVC and GC seismogenic regions.

In our opinion, use of increasing P-wave time windows, validation of the GMPE for large distances considering larger magnitude event recordings, and an upgrade of all networks in the area toward real-time data telemetry capability are primary tasks for the realization of an effective front-detection EEWS in the Iberian Peninsula.

Acknowledgments

We would like to thank K. Fleming for his comments and suggestions that allowed us to significantly improve the manuscript. K. Fleming kindly also improved the English. This work was partially supported by MINECO, projects CGL2010-19803-C03-01 and CGL2013-45724-C3-1 and by the INNOCAMPUS project (Ministerio de Economía y Competitividad, Orden CIN/1934/2010), and the REAKT-Strategies and tools for Real Time Earthquake RisK ReducTion FP7 European project funded

from the European Community's Seventh Framework Programme (FP7/2007–2013) under Grant Agreement No. 282862.

References

Akkar, S. and Bommer, J. J. (2007), *Empirical Prediction Equations for Peak Ground Velocity Derived from Strong-Motion Records from Europe and the Middle East*. Bulletin of the Seismological Society of America, Vol. *97*, No. 2, pp. 511–530, April 2007, doi:10.1785/0120060141.

Alcik, H., O. Ozel, N. Apaydin, and M. Erdik M. (2009). *A study on warning algorithms for Istanbul earthquake early warning system*, Geophys Res. Lett. *36*, L00B05, doi:10.1029/2008GL036659.

Bindi, D., L Luzi, M Massa, F Pacor. (2010) *Horizontal and vertical ground motion prediction equations derived from the Italian Accelerometric Archive (ITACA)*. Bulletin of earthquake engineering *8* (5), 1209–1230.

Böse, M., Ionescu, C., and Wenzel, F. (2007). *Earthquake Early Warning for Bucharest, Romania: Novel and revised scaling relations*. Geophys Res Lett. *34*, L07302.

Böse, M., Hauksson, E., Solanki, K., Kanamori, H. and Heaton, T.H. (2009). *Real-time testing of the on-site warning algorithm in Southern California and its performance during the July 29, 2008 M_w 5.4 Chino Hills earthquake*, Geophys Res Lett. *36* doi:10.1029/2008GL036366.

Böse, M., Heaton, T. and Hauksson, E. (2012). *Rapid estimation of earthquake source and ground-motion parameters for earthquake early warning using data from single three-component broadband or strong-motion sensor*, Bull. Seismol. Soc. Am., *102*(2), pp. 738–750, doi:10.1785/0120110152.

Buforn, E., A. Udías, and M. A. Colombás, (1988a). *Seismicity, source mechanisms and seismotectonics of the Azores-Gibraltar plate boundary*. Tectonophysics, *152*, 89–118.

Buforn, E., A. Udías, and J. Mezcua, (1988b). *Seismicity and focal mechanisms in south Spain*. Bull. Seism. Soc. Am., *78*, 2008–2224.

Buforn, E., M. Bezzeghoud, A. Udías, and C. Pro, (2004). *Seismic sources on the Iberia-African plate boundary and their tectonic implications.* Pure Appl. Geophys. *161*, 623–646, doi:10.1007/s00024-003-2466-1.

Carranza, M., E. Buforn, S. Colombelli, and A. Zollo (2013). *Earthquake early warning for southern Iberia: A P wave threshold-based approach,* Geophys. Res. Lett., *40*, doi:10.1002/grl.50903.

Colombelli, S., Amoroso, O., Zollo, A. and Kanamori, H. (2012a). *Test of a Threshold-Based Earthquake Early Warning Using Japanese Data*, Bull. Seism. Soc. Am., *102*, doi:10.1785/0120110149.

Colombelli, S., A. Zollo, G. Festa, and H. Kanamori (2012b). *Early magnitude and potential damage zone estimates for the great Mw 9 Tohoku-Oki earthquake*, Geophys. Res. Lett., *39*, L22306, doi:10.1029/2012GL053923.

Colombelli, S., Zollo, A. Festa, G. and M. Picozzi (2014). *Evidence for a difference in rupture initiation between small and large earthquakes*. Nat. Commun. *5*:3958 doi:10.1038/ncomms4958.

Espinosa-Aranda, J.M., A. Cuellar, A. Garcia, G. Ibarrola, R. Islas, S. Maldonado, and F.H. Rodriguez (2009*). Evolution of the Mexican Seismic Alert System (SASMEX)*, Seism. Res. Lett. *80* 694–706.

Espinosa-Aranda, J. M., A. Jiménez, G. Ibarrola, F. Alcantar, A. Aguilar, M. Inostrosa, and S. Maldonado (1995). *Mexico City Seismic Alert System*, Seism. Res. Lett., *66*(6), 42–52.

Fernández-Ibáñez, F., Soto, J.I., Zoback, M.D. y Morales, J. (2007): *Present-day stress field in the Gibraltar Arc (western-Mediterranean)*. J. Geophys. Res, *112*:B08404, doi:10.1029/2006JB004683.

Font, Y., H. Kao, S. Lallemand, C.-S. Liu, and L.-Y. Chiao (2004). *Hypocentral determination offshore eastern Taiwan using the maximum intersection method,* Geophys. J. Int. *158*, 655–675.

Fukao, Y. (1973). *Thrust faulting at lithospheric plate boundary. The Portugal earthquake of 1969*. Earth Plan. Sci. Lett. *18*, 205–216.

Grimison, N.L., Chen, W.P., (1988). *Source mechanisms of four recent earthquakes along the Azores–Gibraltar plate boundary*. Geophysical Journal *92*, 391–401.

Hayward, N., Watts, A.B., Westbrook, G.K. and Collier, J.S. (1999): *A seismic reflection and GLORIA study of compressional deformation in the Gorringe Bank region, eastern North Atlantic*. Geophys. J. Int., *138*:831–850.

Horiuchi, S., H. Negishi, K. Abe, A. Kamimura, and Y. Fujinawa (2005). *An automatic processing system for broadcasting system earthquake alarms,* Bull. Seism. Soc. Am. *95*, 347–353.

Iannaccone G, Zollo A, Elia L, Convertito V, Satriano C, Martino C, *et al.* (2009) *A prototype system for earthquake early-warning and alert management in southern Italy*. Bull Earthquake Eng, doi:10.1007/s10518-009-9131-8.

IGN (1983) Sismicidad del Area Ibero-mogrebí. Publicación 203. Presidencia del Gobierno.

Johnston, A. C. (1996). *Seismic moment assessment of earthquakes in stable continental regions, III New Madrid 1811–1821, Charleston 1886 and Lisbon 1755*. Geophys. J. Int., *126*, 314–344.

Martínez Solares, J. M. and A. López Arroyo (2004). *The great historical 1755 earthquake. Effects and damage in Spain*. J. Seismol. *8*, 275–294.

Morel, J.L. y Meghraoui, M. (1996): *Goringe-Alboran-Tell tectonic zone: A transpression system along the Africa-Eurasia plate boundary*. Geology, *24*:755–758.

Kanamori, H. (2005). *Real-Time Seismology and Earthquake Damage Mitigation*, Annu. Rev. Earth Planet. Sci., *33*, 195–214. doi:10.1146/annurev.earth.33.092203.122626.

Peng, H.S., Z.L. Wu, Y.M. Wu, S.M. Yu, D.N. Zhang, and W.H. Huang (2011). *Developing a prototype earthquake early warning system in the Beijing Capital Region*, Seism. Res. Lett. *82* 394–403.

Pro, C., E. Buforn, M. Bezzeghoud, and A. Udías, (2013). *The earthquakes of 29 July 2003, 12 February 2007, and 17 December 2009 in the region of Cape Saint Vincent (SW Iberia) and their relation with the 1755 Lisbon earthquake*. Tectonophysics *583*, 16–27, doi:10.1016/j.tecto.2012.10.010.

Rydelek, P. and S. Horiuchi (2006). *Earth science: is earthquake rupture deterministic?* Nature *442*. doi:10.1038/nature0496 3.

Rydelek, P., C. Wu, and S. Horiuchi (2007). *Comment on Earthquake magnitude estimation from peak amplitudes of very early seismic signals on strong motion records by Aldo Zollo, Maria Lancieri, and Stefan Nielsen.* Geophys. Res. Lett. *34*. doi:10.1029/2007GL029387.

Satriano, C., A. Lomax, and A. Zollo (2008). *Real-Time Evolutionary Earthquake Location for Seismic Early Warning*. Bulletin of the Seismological Society of America America *98*.3, pp. 14821494. doi:10.1785/0120060159.

Satriano, C., Elia, L., Martino, C., Lancieri, M., Zollo, A., and Iannaccone, G. (2011). *PRESTo, the earthquake early warning system for southern Italy: concepts, capabilities and future perspectives, Soil Dyn*. Earthq. Eng. *31*, 137–153. doi:10.1016/j.soildyn.2010.06.008.

Stich, D., F. Mancilla, S. Pondrelli, and J. Morales (2007). *Source analysis of the February 12th 2007, Mw 6.0 Horseshoe earthquake: Implications for the 1755 Lisbon earthquake*. Geophysical Research Letters *34*. doi:10.1029/2007GL0300127.

Udías, A., López Arroyo, A., Mezcua, J., 1976. Seismotectonic of the Azores-Alboran region. Tectonophysics *31*, 259–289.

Wald, D. *et al.* (1999). *Relationships between Peak Ground Acceleration, Peak Ground Velocity, and Modied Mercalli Intensity in California.* In: Earthquake Spectra *15*.3, p. 557. doi:10.1193/1.1586058.

Wu, Y.M. and L. Zhao (2006). *Magnitude estimation using the first three seconds P-wave amplitude in earthquake early warning*, Geophys Res Lett. *33*, L16312, doi:10.1029/2006GL026871.

Wu, Y.-M. and H. Kanamori (2005). *Rapid Assessment of Damage Potential of Earthquakes in Taiwan from the Beginning of P - Waves*. Bulletin of the Seismological Society of America America *95*.3, pp. 1181–1185. doi:10.1785/0120040193.

Wu, Y.-M. and H. Kanamori (2008a). *Development of an earthquake early warning system using real-time strong motion signals*. Sensors *8*, pp. 1–9.

Wu, Y.-M and H. Kanamori (2008b). *Exploring the feasibility of on-site earthquake early warning using close-in records of the 2007 Noto Hanto earthquake*. Earth Planets and Space *60*, pp. 155–160.

Zollo, A., M. Lancieri, and Nielsen, S. (2006). *Earthquake magnitude estimation from peak amplitudes of very early seismic signals on strong motion*, Geophys Res Lett. *33*, L23312, doi:10.1029/2006GL027795.

Zollo, A., M. Lancieri, & Nielsen, S. (2007). Reply to comment by P. Rydelek et al. *On Earthquake magnitude estimation from peak amplitudes of very early seismic signals on strong motion records*. Geophysical Research Letters *34*.20, pp. 1215. doi:10.1029/2007GL030560.

Zollo, A, O. Amoroso, M. Lancieri, Y.M. Wu and Kanamori, H. (2010). *A threshold-based earthquake early warning using dense accelerometer networks*, Geophys J Int *183* 963–974.

Zollo, A., S. Colombelli, L. Elia, A. Emolo, G. Festa, G. Iannaccone, C. Martino, and P. Gasparini (2014). An integrated regional and on-site Earthquake Early Warning System for Southern Italy: concepts, methodologies and performances, In "Early Warning for Geological Disasters—Scientific methods and current practices", Eds Wenzel & Zschau, Springer.

(Received July 18, 2014, revised November 28, 2014, accepted December 5, 2014)